SLAC-PUB-11007
January 2005

Impedance Calculation and Verification in Storage Rings *

Karl L.F. Bane, SLAC, Menlo Park, CA 94025, USA
Katsunobu Oide, KEK, Tsukuba, Japan
Mikhail Zobov, INFN, Frascati, Italy

Abstract

For both the SLC damping rings and the DAΦNE collider a systematic approach to understanding single bunch, longitudinal, current dependent behavior was taken: First, using a bunch significantly shorter than nominal, a careful calculation of the wakefield of the entire vacuum chamber was obtained. This "pseudo-Green" function was then used in bunch lengthening and instability calculations. We review, for both projects, the history of these calculations and comparisons with measurement.

Presented at the CARE-HHH-APD Workshop on Beam Dynamics in Future Hadron Colliders and Rapidly Cycling High-Intensity Synchrotrons (HHH 2004), CERN, Geneva, Switzerland November 8-11, 2004

*Work supported by Department of Energy contract DE–AC02–76SF00515.

IMPEDANCE CALCULATION AND VERIFICATION IN STORAGE RINGS

Karl L.F. Bane*, SLAC, Menlo Park, CA 94025, USA
Katsunobu Oide, KEK, Tsukuba, Japan
Mikhail Zobov, INFN, Frascati, Italy

Abstract

For both the SLC damping rings and the DAΦNE collider a systematic approach to understanding single bunch, longitudinal, current dependent behavior was taken: First, using a bunch significantly shorter than nominal, a careful calculation of the wakefield of the entire vacuum chamber was obtained. This "pseudo-Green" function was then used in bunch lengthening and instability calculations. We review, for both projects, the history of these calculations and comparisons with measurement.

INTRODUCTION AND CONCLUSION

In designing an electron storage ring one important consideration is the longitudinal, broad-band impedance of the vacuum chamber, and the effects of this impedance on single bunch behavior of the beam. Possible effects include: potential well bunch lengthening, a threshold current, and—above threshold—energy spread increase and bursting ("saw-tooth") behavior. Any of these behaviors may be deleterious to the performance of a collider, light source, or storage ring, and may need to be avoided.

In particular, for stable, reliable operation it is often desirable that the threshold to the instability be above the operating current. The analysis of stability of a ring normally begins (and often ends) with the Boussard criterion [1]:

$$\frac{e\hat{I}|Z(n)/n|}{2\pi\alpha E\sigma_\delta^2} \leq 1 \quad , \tag{1}$$

with $\hat{I}$ the peak current within the bunch, Z the longitudinal (broad-band) impedance, $n = \omega_1/\omega_0$ where ω_1 is a typical bunch frequency and ω_0 is the revolution frequency, α is momentum compaction, E is energy, and σ_δ is relative energy spread in the beam. Typically, the impedance is calculated for a few important vacuum chamber objects, the contributions are added together, and then inserted into the Boussard equation to estimate the threshold current.

In the studies on the damping rings of the Stanford Linear Collider (SLC) and the DAΦNE collider a new, more systematic approach was used. In both cases, starting with drawings of the vacuum chamber components, an accurate wakefield representing the entire ring was numerically obtained. The driving bunch in the calculations was only a fraction in length of the nominal bunch length, allowing one to use the wake as a pseudo-Green function in subsequent potential well and instability calculations. No adjustable parameters nor fitting was used. In the following two sections we give the history of the calculations and comparisons with measurement for the SLC damping rings and for DAΦNE.

In reading these two sections we see that our approach was quite successful in reproducing measured data (though not perfectly), allowing us to make predictions and obtain insights into the longitudinal, current dependent behavior of the beam. Agreement was found for the current dependence of bunch shape (especially good agreement in the case of DAΦNE), bunch length, synchronous phase; for the threshold current, and—above threshold—the oscillation frequency of the instability. The calculations defined the design strategy of almost all principal vacuum chamber components—in the case of DAΦNE, and led to a redesign of the entire vacuum chamber—in the case of the SLC. Also, through the work of the SLC damping rings a new instability (the *weak* instability) was discovered, triggering theoretical work to understand it. Note, by the way, that the Boussard criterion often has only an order of magnitude value, and it has nothing to say about the weak instability.

Our approach to impedance calculations appears to have been quite successful; so it is somewhat surprising that it has been seldom used since, and then typically with little success. For example, at the ATF storage ring at KEK the same approach to calculations was followed; nevertheless, bunch length measurements indicate that there is a large amount of still unaccounted for impedance in the ring [2]. It may be that, given the complicated nature of some vacuum chamber components, calculations as described here can still be somewhat of an art form, and one not guaranteed of easy success.

The subject of this report was to be "Impedance Codes and Benchmarking." By "benchmarking" one can, for example, mean comparing the results of programs, comparing impedance calculations with bench measurements, or (the meaning we pursue) the calculation of ring wakes and consequent current dependent behavior, and then comparison with measurement in the ring. Three types of codes are used in such analysis: impedance (wakefield) calculation codes, threshold finding through a perturbation solution of the Vlasov equation, and tracking for studying behavior above threshold. The programs used (described in the text) seem to have been up to the task for the SLC damping rings and for DAΦNE. However, for all three categories there are recent improvements that should aid the next generation of designers.

In wakefield calculations with short bunches and long structures, the so-called "mesh dispersion" can result in totally wrong results when straightforward calculation is pursued. A. Novokhatski, *et al*, for cylindrically symmetric structures [3], and more recently Zagorodnov and Weiland,

* Work supported by the Department of Energy, contract DE-AC02-76SF00515

for 3D structures [4], have developed methods to alleviate this problem. The Oide Vlasov equation solver gives a forest of stable modes (an artifact) amidst any unstable mode one might be searching for [5]. R. Warnock, *et al*, have reformulated the problem to avoid this artifact [6]. Also, the Oide method, for some impedances, simply fails; the new method seems to have more chance of success (though it can also fail) [7].

As for studying behavior above threshold, R. Warnock and J. Ellison have recently developed a program that solves the Vlasov-Fokker-Planck (VFP) equation, that is more accurate than simple macro-particle tracking [8]. It can, for example, solve also for a coherent synchrotron radiation (CSR) driven, microbunching instability (it appears that such an instability has been observed, *e.g.* at BESSY II [9]), which is likely impossible to treat with simple tracking. Comparison with measurements of the saw-tooth behavior in the SLC (described in the text) shows promise that one can explore even such complicated behavior numerically with some accuracy.

In the Appendix of this report we present our Panel Comments given at the CARE-HHH workshop held at CERN in November 2004.

SLC DAMPING RINGS

Introduction

In the Stanford Linear Collider (SLC) the beam, after leaving the gun, was stored a few damping times in a damping ring, compressed in the ring to linac (RTL) transfer line, accelerated in the linac, turned around in the arcs, and collided with the opposing beam in the interaction region. Soon after commissioning of the collider it was realized that, in the damping rings, the threshold (single bunch) current to the longitudinal microwave instability was very low. Above threshold, there was small pulse-to-pulse variation in bunch length and longitudinal phase of the extracted beam, that was amplified in the linac, and that made it almost impossible to operate the collider.

The SLC damping ring vacuum chambers seem to have been designed with little concern as to their impedance effects. Or it may have been that, at the time, small vacuum chamber objects and transitions were not considered especially dangerous from an impedance point of view. At about the same time (the early 1980's) an impedance upgrade to SPEARII involved removing from the ring large objects, such as RF cavities and beam separators, with seemingly little concern for smaller objects. (This left the ring more inductive, resulting in longer bunches, which is probably why mini-beta failed to increase the luminosity [10].) It turned out (as we will show) that for the SLC damping rings it was, indeed, small objects that dominated the original impedance.

The SLC damping ring vacuum chamber has had three incarnations. After beginning operation with the *original* chamber, when the microwave instability was recognized as limiting performance (in the late 1980's), the bellows were sleeved, resulting in the *old* chamber. In 1994 the entire chamber in both rings was removed, and a new, low impedance vacuum chamber was installed (the *current* or *new* chamber).

In this report we present, in chronological order for all three versions of vacuum chambers, the original calculations of the impedance and its expected effect on the beam, and the comparison with measurement. At the time the calculations were done we were somewhat limited by computing power and programs for calculating wakefields; much better calculations were possible already by the time of DAΦNE (described in the next section), and even more is possible today. Nevertheless, even with our sometimes crude calculations we were able to reproduce (admittedly, at times in hindsight) many important features of bunch lengthening and the microwave instability found in measurement, and also to provide insight into the physics behind this complicated phenomenon.

The original impedance calculations come from Ref. [11],[12], for the original/old rings, Ref [13] (with C.-K. Ng) for the new ring. The instability calculations can be found in Refs. [14] (old ring) and [15] (new ring). We apologize that many figures are not clear; their originals could not be found, and they were extracted from pdf files of reports. Selected SLC damping ring parameters are given in Table 1.

Table 1: Selected SLC damping ring parameters. Note that, sometime after the new ring chamber was installed, the nominal bunch length and energy spread were increased (by 6%), and the damping time reduced, by a modification of the damping partition numbers [16].

Parameter	Value	Units
Energy	1.15	GeV
Circumference	35	m
Typical beam pipe radius	1	cm
RF frequency	714	MHz
Nominal RF voltage	0.8	MV
Nominal rms bunch length	5	mm
Nominal rms energy spread	0.07	%
Nominal synchrotron frequency	99	kHz
Synchrotron radiation damping time	1.7	ms

Original vacuum chamber

The study of the SLC damping ring impedance began with blueprints of the vacuum chamber, to obtain dimensions, which were then used to calculate wakefields. We felt it was better to start from first principles than use simplified models, such as the $Q = 1$ resonator model (see *e.g.* [17]), as is sometimes done. The goal of the impedance calculations was to obtain two things: (i) an understanding of the relative importance of various objects, and (ii) a pseudo-Green function wake—that represents, as accurately as possible, the interaction of all objects—that can be used in potential well, threshold, and tracking simulations.

The original ring vacuum chambers were composed of 40, essentially cylindrically symmetric, quad chamber segments (20 each of “QF” or “QD” type), separated by bend chambers with a rather rectangular cross-section (see Fig. 1). The quad segments are sketched in Fig. 2. We see bend-to-quad transitions, cavity-type beam position monitors (bpms), bellows, masks, and flex joints. The ring also has special chambers that include such things as 2 two-cell rf cavities, kickers, septa, y-joints, etc.

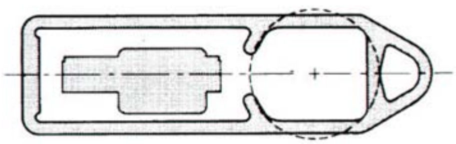

Figure 1: Cross-section of a bend chamber. The dashed circle shows the size of a quad chamber beam pipe.

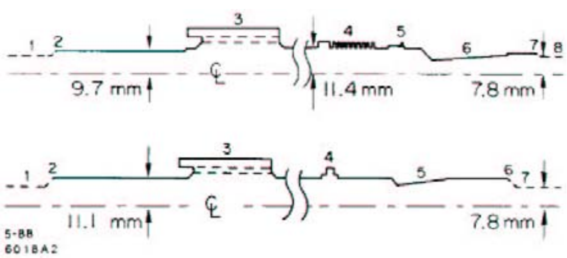

Figure 2: Vertical profile of QF segment (top) and QD segment (bottom). Non-cylindrically symmetric parts are indicated by dashes.

The characterization of a ring impedance as inductive, resistive, or capacitive comes from electrical circuit analogies (an early usage was by Haïssinski [18]). A ring can be said to be inductive if the induced voltage can be written as $V_{ind} \approx -L\, dI/dt$, with $I(t)$ the bunch current and L a constant (the inductance), and it can be characterized as resistive if $V_{ind} \approx -RI$, with R a constant (the resistance), etc. An inductive ring means potential well bunch lengthening and increased tune spread with current, a resistive ring has little of either (see, *e.g.* Refs. [12],[19]). Individual vacuum chamber objects can often also be characterized as inductive, resistive, etc. Small objects or gradual perturbations—bellows, masks, transition—tend to be inductive at normal bunch lengths; larger objects, such as RF cavities and cavity beam position monitors (bpm’s), tend to be resistive or have large resistive components. Note that for most vacuum chamber objects these simple models, at best, only approximately describe their wakefields.

Wakefields of vacuum chamber objects in the SLC damping rings were obtained using early versions of MAFIA2D and MAFIA3D, which are finite difference mesh programs that compute the wakefield of a gaussian bunch in the time domain [20]. For the many inductive objects in the SLC damping ring the wake was calculated for a nominal bunch and then fit for the effective inductance L. A table of inductive objects in the original SLC damping ring is given in Table 2. At the time that these calculations were done it was difficult to use a fine enough mesh to obtain an accurate result for some 3D objects; instead, a 2D calculation was performed, with an azimuthal filling factor (the ”Factor” in the table) used to approximate the 3D result. Nowadays this is not generally necessary. Nevertheless, the results in the table indicate that the dominant contributors to the impedance were the bellows, the masks, and the transitions. The total inductance, 50 nH, equivalent to $|Z/n| = 2.6\ \Omega$, was very large. The rf cavities are resistive, with an effective resistance of 411 Ω.

Table 2: Inductive vacuum chamber objects in the *original* SLC damping rings.

Single Element Inductance		Contribution in Ring		
Type	L/nH	Factor	Number	L/nH
QD bellows*	0.62	1.0	20	12.5
QD and QF masks	0.47	1.0	20	9.5
QD & QF trans.	0.52	0.9	20	9.3
ion pump slots	1.32	0.1	40	5.3
kicker bellows*	2.03	1.0	2	4.1
flex joints	0.18	1.0	20	3.6
1” bpm trans.	0.10	0.8	40	3.3
other				2.4
			Total	50.0

*Shielded in the late 1980’s by the addition of sleeves.

To obtain the pseudo-Green function wake, calculations were performed using a $\sigma_z = 1$ mm gaussian bunch. To properly account for the interaction of neighboring vacuum chamber objects the QF and QD segments—containing the most important impedance objects—were each calculated as one piece. As far as obtaining an accurate Green function, we were fortunate that the dominant contributions came from (essentially) cylindrically symmetric chambers that were repeated many times. The most difficult-to-calculate objects, such as the septa and y-joints, were and could be left out. The Green function wake for the original ring is shown in Fig. 3.

Convolving (minus) the Green function with a 6 mm gaussian bunch we obtain the bunch wake shown in Fig. 4 (here a negative value indicates voltage loss). We see that, though largely inductive, the ring wake has a significant resistive component. Performing the Fourier transform of the Green function we obtain the impedance; we find that $|Z/n|$ rises to a maximum at 15 GHz (above cut-off) due to the bellows, and then drops to become numerical noise beyond 30 GHz (see Fig. 5). We see that, by simply shielding the bellows, the impedance can be significantly reduced (the dots in the figure give the remaining impedance).

To obtain the steady-state bunch shape below threshold

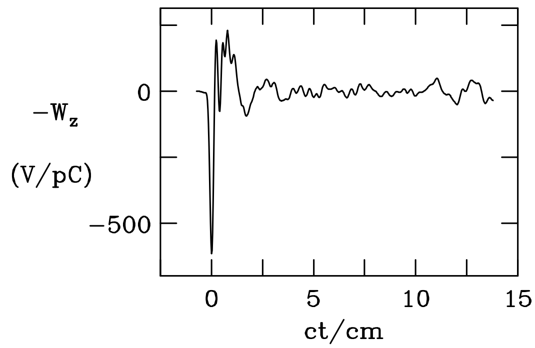

Figure 3: Pseudo-Green function for the *original* SLC damping ring: the wake of a $\sigma_z = 1$ mm gaussian bunch. A positive value indicates voltage loss for a test particle.

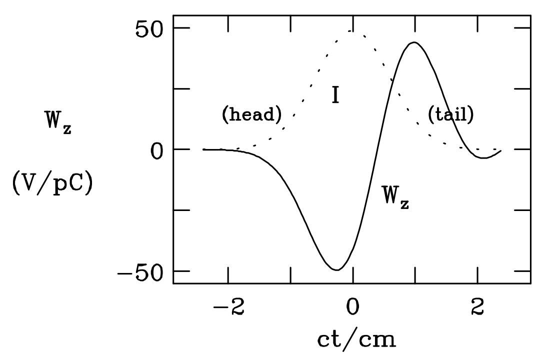

Figure 4: Convolution of minus the Green function wake with a 6 mm gaussian bunch. The bunch shape is indicated by dots.

we used the Green function and numerically solved the Haïssinski equation [18]. To get the average shape above threshold, we used the same method but first scaled the nominal bunch length parameter σ_{z0} by the energy spread increase, as obtained from measurements (described below). The scaling turns out to be $\sim N^{1/3}$.

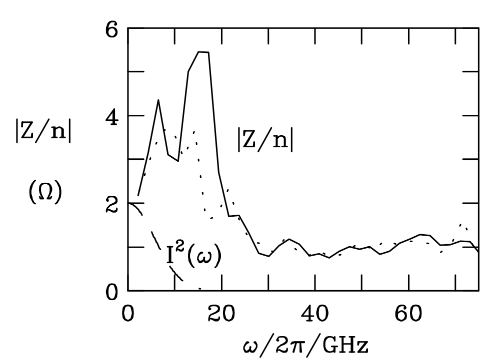

Figure 5: The impedance $|Z/n|$. The dots give what remains when the bellows are shielded (the *old* ring impedance). The power spectrum of a 6 mm bunch is also shown.

Measurement [21] During SLC operation the beam, once extracted from the ring, passed through the ring-to-linac (RTL) transfer line on its way to the linac. Using a digitized phosphor screen located in a dispersive region of the RTL one could measure the energy spread or—after inducing a longitudinal-energy correlation in the beam—the bunch length of the beam. The current-dependent centroid shift or, equivalently, the parasitic mode losses, were obtained by measuring the RF component of a bunch intensity signal as the beam current was gradually scraped away.

The measured bunch length, energy spread, and centroid shift as functions of bunch population are shown in Fig. 6. The energy spread appears to be independent of current up to $N_{th} = 1.5 \times 10^{10}$, and then increases as $\sigma_E \sim N^{1/3}$. We note that bunch lengthening (frame a) is quite pronounced: the full-width-at-half-maximum (FWHM) length, z_{fwhm} has doubled by $N = 3 \times 10^{10}$. The fact that $z_{fwhm} > 2.355\sigma_z$ (σ_z is rms length) indicates that the beam is more bulbous than a gaussian, which is consistent with an inductive impedance [19]. The potential well calculations are given by lines in Figs. 6 (dashed lines above threshold); we see good agreement with measurement. in Fig. 7 we present selected measured bunch shapes (the plotting symbols) and their comparison with calculation (the lines).

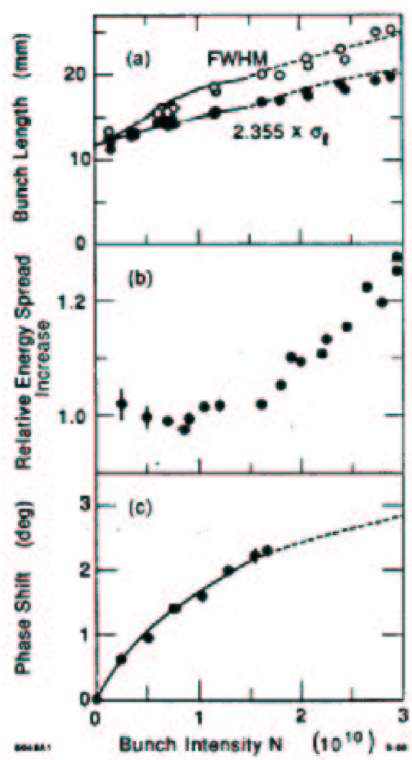

Figure 6: For *original* ring, bunch length (both full-width-at-half-maximum and 2.355 times rms length) (a), energy spread (b), and centroid shift (c) as functions of bunch population. Lines are calculations and plotting symbols are measurement data. From Ref. [21].

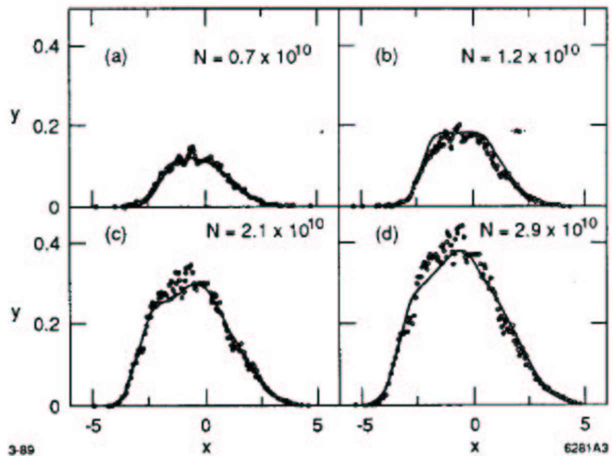

Figure 7: Bunch shape (head is to left) for several currents. Abscissae are position normalized to $\sigma_{z0} = 5$ mm; ordinates are $IZ_0/(V'\sigma_{z0})$ ($Z_0 = 377\ \Omega$, V'_{rf} is the slope of the RF voltage). Lines are calculations and plotting symbols are measurement.

Old ring

In the original SLC damping rings, the microwave instability was encountered at $N = 1.5 \times 10^{10}$. Our simulations showed that the bellows were a dominant impedance source, and that the instability threshold could be increased a factor of 2 by shielding them. Sleeves were inserted in the bellows of both rings. This version of the machine we call the *old* ring.

Shielding the bellows also made the ring somewhat less inductive, reducing the estimated strength of inductors from 50 nH to 33 nH. Again a Green function was generated and potential well calculations were performed; the calculated bunch length with current was not very different from before. In addition, macro-particle tracking of longitudinal phase space was performed, in order to simulate the beam behavior above threshold [22]-[26]. In this calculation the longitudinal position and energy of a few hundred thousand macro-particles were tracked. On each turn, each particle's energy was modified to include effects of the RF wave, Robinson damping, quantum excitation, radiation damping, and the wakefield; and then each particle's position was modified through the momentum compaction factor.

A tracking example using the old ring Green function is given in Fig. 8. Shown is the turn-by-turn (N_t is turn number) skew moment of the bunch shape when $N = 3.5\times10^{10}$ (a), and the rms length when $N = 5.0\times10^{10}$ (b). In the simulations 300,000 macro-particles were used. To keep the computer running time reasonable, the synchrotron radiation damping time was artificially reduced from 15,000 turns by a factor of 10 (in the old ring the results were not very sensitive to the damping time). The synchrotron period was 85 turns. We see from the results that for some currents a "saw-tooth" like behavior in the rms length is obtained.

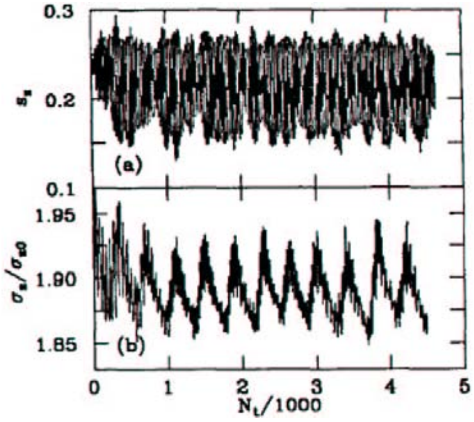

Figure 8: For *old* ring, turn-by-turn (N_t is turn number) skew moment when $N = 3.5 \times 10^{10}$ (a), and the rms when $N = 5.0 \times 10^{10}$ (b).

The Fourier transform (FT) of the turn-by-turn skew moment of the calculations for the same two currents is given in Fig. 9. At some currents, such as at $N = 3.5 \times 10^{10}$, we obtain an extremely narrow resonance. The position of the peaks of the resonance in the Fourier transform, normalized to the synchrotron tune, as function of N is plotted Fig. 10. Beginning with a calculated threshold $N_{th} = 2 \times 10^{10}$ the resonance frequency grows from $2.5\nu_{s0}$ (ν_{s0} is nominal synchrotron tune) nearly linearly with slope $0.27\nu_{s0}/10^{10}$.

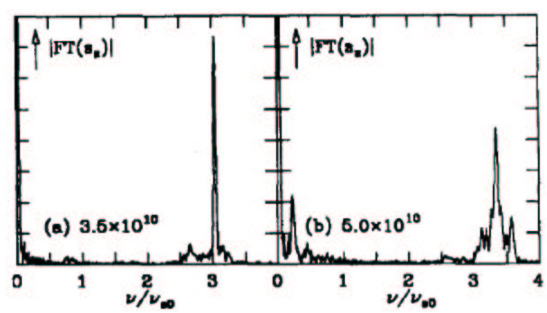

Figure 9: The absolute value of the Fourier transform of the turn-by-turn skew moment for two currents.

In Fig. 11 we present the bunch shape at extrema of the mode oscillation, when $N = 3.5 \times 10^{10}$ (the dashed curves give the average, Haïssinski distribution). In Fig. 12 we give the shape in phase space of the unstable mode at $N = 3.5 \times 10^{10}$. This was obtained by averaging the phase space distribution at a fixed phase in the oscillation and subtracting from it the average over all phases. We see that the mode is not simple; rather it is a complex mixture of dipole, quadrupole, and sextupole components, which we believe is a consequence of the strongly inductive (though not purely inductive) nature of the ring.

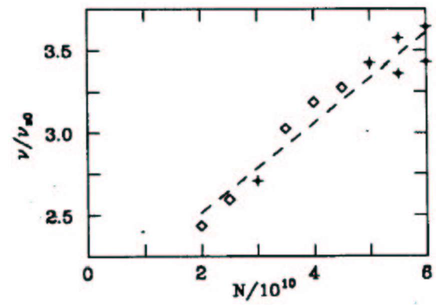

Figure 10: The positions of the major peaks in the Fourier transform of the skew moment, normalized to the synchrotron tune, *vs.* N.

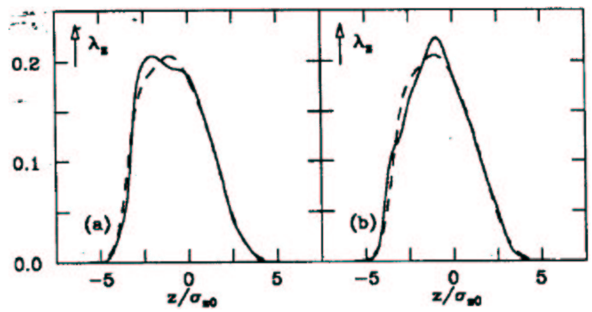

Figure 11: For *old* ring, the bunch shape at extrema of the mode oscillation, when $N = 3.5 \times 10^{10}$ (the dashed curves give the average, Haïssinski distribution). The head is to the left.

Vlasov equation calculation Another program useful for understanding a longitudinal, microwave instability was written by one of us (K.O.); it solves the time independent, linearized Vlasov equation including the effects of potential well distortion; we will refer to it here as "the Oide Vlasov solver" [5]. The authors end up with an infinite dimensional, linear matrix eigenvalue problem that is truncated to finite size. For a given current the problem is solved, and the appearance of an eigenmode with complex eigenvalue indicates an unstable mode. The program is used to find the threshold, and also the shape and frequency of the unstable mode. One can also approximately go beyond threshold by assuming the average energy distribution remains gaussian, with the rms energy spread increasing to keep the beam just at threshold.

Using the old SLC damping ring Green function, the first unstable mode the program found was at $N = 1.9 \times 10^{10}$ with a frequency of $2.5\nu_{s0}$, and the shape of the mode was also similar to that found by the macro-particle tracking program. Due to the strongly inductive nature of the ring, and its attendant large tune spread, already at $N = 0.5 \times 10^{10}$ modes with different azimuthal and radial mode numbers overlap in frequency; at threshold the instability cannot be described as the collision of two simple modes (*a la* mode coupling theory [27]).

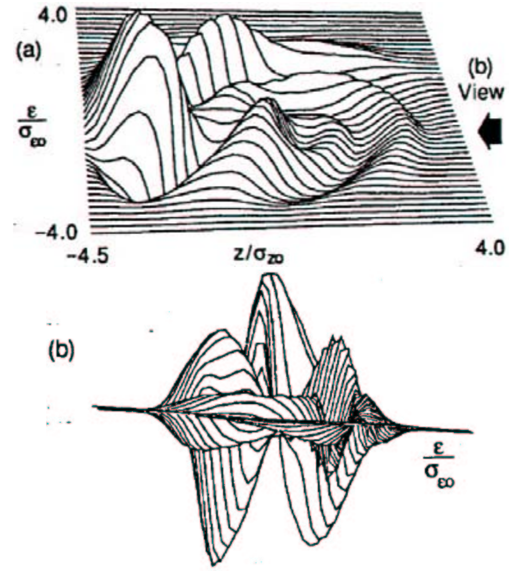

Figure 12: For old ring, the shape of the unstable mode from two views at $N = 3.5 \times 10^{10}$.

Measurement [28] After the bellows were sleeved the measured bunch length was similar to that of the original ring, only 10% shorter at $N = 3 \times 10^{10}$. The threshold increased by a factor of two to $N_{th} = 3 \times 10^{10}$. At threshold, on a spectrum analyzer set to a revolution harmonic near 20 GHz, a sideband with a frequency shift of $2.5\nu_{s0}$ was observed (the "sextupole" mode); at higher current the frequency shift increased. A second, weaker sideband was found at about twice the frequency of the first one.

At certain currents above threshold, a repeating sequence of growth and relaxation was observed on beam phase and bunch length signals of the stored beam. The growth time was on the order of the synchrotron period, and the relaxation time on the order of the damping time (the "saw-tooth"). A parameter study over RF voltage and beam current found what might be called phase transitions, with different regions of parameter space displaying qualitatively different types of behavior (the "Nose Plot" [29],[30]). For example, under some conditions the saw-tooth disappeared completely, to be replaced by even oscillations.

Comparing with calculations, the measured bunch length with current was still in good agreement. The measured threshold had increased by a factor of two (as in calculation), though the absolute value was still 50% larger than calculated. The slope of the "sextupole" mode frequency with current was in good agreement [31]; the second sideband, however, was not seen in simulation. Also, although continuous oscillation and sawtooth above threshold could both be found in tracking simulations, we would not say that the calculated saw-tooth convincingly corresponded to measurement. Finally, note that the discovery of the saw-tooth instability in the SLC damping rings engendered much theoretical interest; see *e.g.* Ref. [32].

Current ring

It was practically impossible to operate the SLC beyond threshold $N_{th} = 3 \times 10^{10}$ because of the microwave instability. An additional problem with the impedance was that, at higher currents, the bunch length extended beyond the linear region of the RTL compressor RF wave, and bunch compression became inefficient. So in 1994 a completely new, low impedance vacuum chamber was installed in both rings. The magnets were not changed, so that quad-to-bend transitions were still needed, but the new ones were much smoother (see Fig. 13); the cavity style bpm's were also not changed. This version of the ring we call here the *current* or *new* ring.

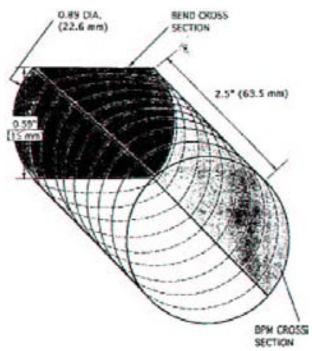

Figure 13: The new, smoother quad-to-bend transitions of the *current* damping ring vacuum chamber. From Ref. [13].

According to our calculations the impedance of the inductive elements for the old ring was 33 nH; with the new chamber inductive elements were eliminated as much as possible, and we estimated the residual inductance at 6 nH [13]. The vacuum chamber had changed character and become resistive. The new Green function wake is shown in Fig. 14. In Fig. 15 we give an example potential well calculation with this wake. We see that the induced voltage is, to good approximation, proportional to the bunch shape. The dashed curve gives the potential well result for a purely resistive impedance with $R = 880\ \Omega$, which we see gives almost the same bunch shape.

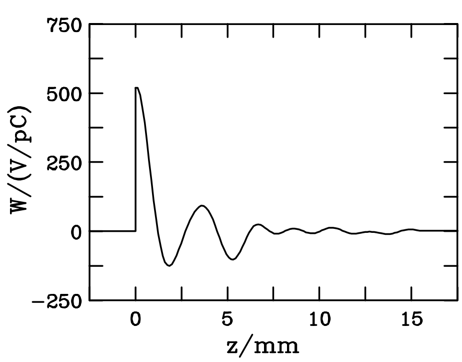

Figure 14: The Green function wake representing the *current* SLC damping rings.

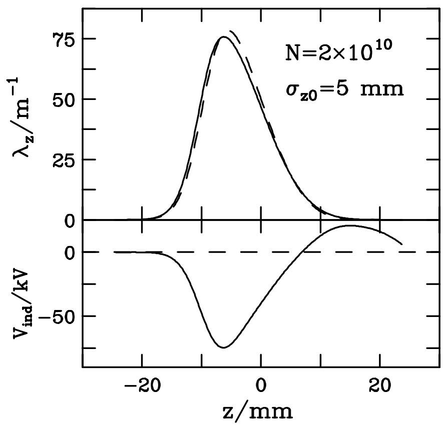

Figure 15: A potential well calculation example using the current ring wake, showing the bunch shape λ_z (the head is to the left) and the induced voltage V_{ind}.

Calculations with the new wake predicted a shorter bunch, and according to particle tracking (again with the damping time artificially reduced by a factor of 10) the threshold appeared to move to $N = 5 \times 10^{10}$. When the new machine was turned on, it was found that bunch lengthening was indeed reduced; the threshold, however, also went down (which came as a shock).

Weak instability About the same time one of us (K.O.) was studying the microwave instability in a ring with an idealized resistive plus inductive impedance [33]; it was found that a machine with a purely resistive impedance is unstable at any current. Unlike F. Sacherer's mode coupling instability, which can be described as two modes with different azimuthal mode numbers colliding, this new type of instability can be described as the collision of two modes with identical azimuthal mode numbers but different radial mode numbers. A simple, double water bag model that describes this type of instability was also developed [34]. Unlike the normal mode coupling instability, it is a weak instability, in that it can be suppressed by a small amount of tune spread—as would be introduced by adding a small amount of inductance to the ring—through Landau damping. We call this instability *weak* as opposed to F. Sacherer's *strong* instability. K.O.'s study suggested that the instability in the new SLC damping ring might be such a weak instability, and our subsequent simulations supported this idea.

Simulations Unlike the old, strong SLC damping ring instability, a weak instability is very sensitive to damping time; this parameter, therefore, could not be artificially lowered in simulations of the new ring to save computing time*. To keep the total running time manageable, the number of macro-particles instead was reduced by a factor

*It was one of us (K.B.) who had not checked this point in the earlier, new damping ring simulations. The redeeming feature of this mistake is that, had we known beforehand that the threshold would be reduced, we might not have built the new chambers, and consequently not have achieved the later, improved luminosities.

of 10—to 30,000—as compared to before. Below threshold and to find threshold this worked fine; above threshold, however, the combination of small number of macro-particles, long damping time, and type of impedance resulted in large fluctuations. This can be seen in Fig. 16, where we plot the turn-by-turn rms energy spread just above threshold (a), and at a higher current (b). Even though there are large fluctuations in the moments of the beam distribution above threshold, we took the average result over the last damping time to estimate the expected average property.

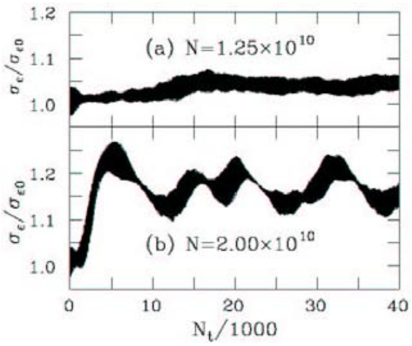

Figure 16: The turn-by-turn rms energy spread obtained by tracking, just above threshold (a) and at a higher current (b).

According to macro-particle tracking the threshold $N_{th} \approx 1.15 \times 10^{10}$, but the result is very sensitive to inductance. By adding a small inductance of 2 nH ($|Z/n| = 0.1\ \Omega$) to the impedance, the threshold can be raised by 1×10^{10} (in agreement with Ref. [33]). When artificially changing the damping time τ_d, we find that $N_{th} \sim \tau_d^{-1/2}$, which implies a growth $\sim e^{\alpha N^2 t}$ (α a constant, t time), also in agreement with Ref. [33]. The threshold and the average beam properties as functions of current above threshold are in good agreement with the Vlasov equation results. The unstable mode is clearly a quadrupole mode (see Fig. 17). The unstable mode frequency is just under $2\nu_{s0}$ at threshold, and then varies with a slope of $-0.07\nu_{s0}/10^{10}$.

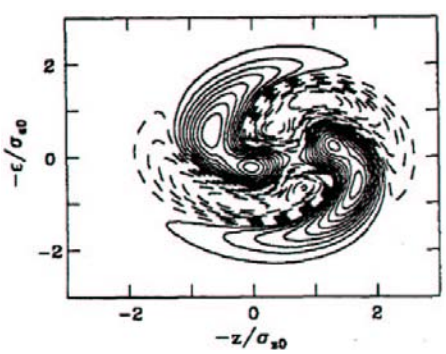

Figure 17: Unstable mode shape at $N = 2 \times 10^{10}$ as obtained by the Vlasov method. The bunch head is to the right, higher energy is down.

Measurement [35] The impedance effects in the current damping ring have been extensively studied through measurement, resulting in one, and the significant part of another, PhD.: for bunch length measurements, primarily using a streak camera [36], and for a detailed study of the properties of the unstable mode above threshold [16]. Bunch length measurements clearly showed that bunch lengthening had been reduced by the introduction of the new chambers (see Fig. 18). The threshold was found at $N_{th} = 1.5$–2×10^{10}. Bunch length and synchronous phase were in good agreement with calculations (when 2 nH inductance was added to our Green function); the bunch shape was found to be consistent with a resistive impedance, and in agreement with calculation. The unstable mode, at threshold, had a frequency of $1.77\nu_{s0}$, and varied with current with a slope of $-0.06\nu_{s0}/10^{10}$, also in good agreement with calculation.

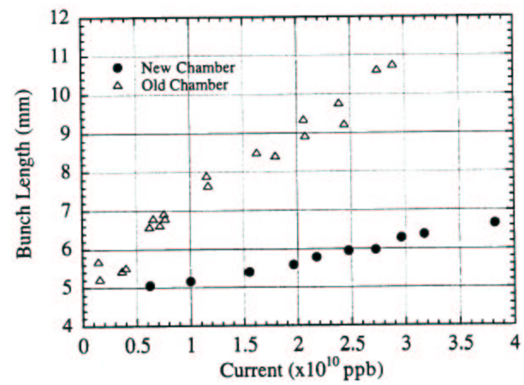

Figure 18: Bunch length (FWHM/2.35) *vs.* current measurements, comparing the new with the original (here called "old") chambers. The new measurements were performed using a streak camera. From Ref. [36].

Measurements of time dependent (saw-tooth) behavior for different currents are shown in Fig. 19. The instability involved the movement from the equilibrium shape of only a few percent of beam particles [16]. It appears that the amplitude of instability in the new ring was less than in the old (old ring saw-tooth measurements were not calibrated), since with the old ring we were limited to threshold, but with the new ring we ran routinely at more than twice threshold, at $N_{th} = 4.5 \times 10^{10}$.

Discussion

Recent programs for calculating impedances/wakefields and for tracking longitudinal phase space in storage rings are much improved. We would briefly like to mention one: a numerical method for solving the Vlasov-Fokker-Planck equation for longitudinal phase space in storage rings has been developed by Ellis and Warnock [8]. The program seems better able to avoid fluctuations in beam properties above threshold that we found *e.g.* with macro-particles in Fig. 16b. Their program was applied to our Green function wakes for the old and current SLC damping ring vac-

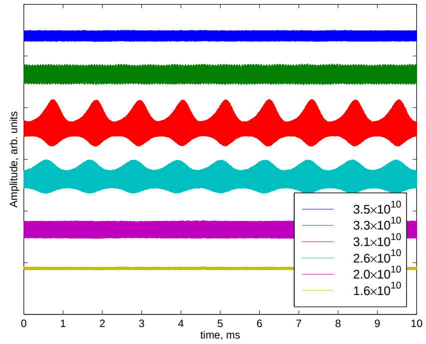

Figure 19: Oscilloscope traces for various currents. The third curve from the top is $N = 3.1 \times 10^{10}$. From Ref [16].

uum chambers [8],[37]. Generally, one can say that there is much agreement between the results of this program and the tracking results presented earlier.

As far as saw-tooth behavior is concerned, it seems that the simulated results can be very sensitive to machine and beam parameters. It may be too much to ask from simulations that they exactly mimic saw-tooth behavior in a real storage ring. Thus Warnock and Ellis find that, although threshold to bunch lengthening, frequency of bunch oscillations, and the period of bursting envelope are in good agreement with measurement for the new ring, other properties are not (*e.g.* the saw-tooth behavior does not disappear again at higher currents, as seen in Fig. 19). An example with agreement: in Fig. 20 we see a simulated oscilloscope trace, obtained by the program, which is meant to be compared to the third curve from the top in Fig. 19.

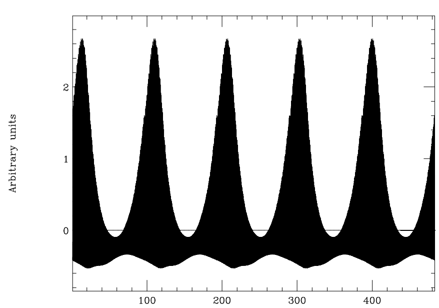

Figure 20: Simulated oscilloscope traces for $N = 3.0 \times 10^{10}$. From Ref. [8].

So finally, how can we understand the reduction of the measured threshold when the SLC damping ring impedance was reduced? In the old, inductive machine there was a strong instability observed at $N_{th} = 3 \times 10^{10}$, and we expect to have increased this threshold when the impedance was reduced. However, in an inductive machine there is a large incoherent tune spread that will Landau damp weak instabilities which might otherwise appear at lower currents. By removing mostly inductive elements, and thereby changing the character of the ring to a resistive one, we have removed this tune spread, and presumably are now able to observe one of these weaker instabilities.

If one could reduce a ring impedance by a scale factor, α, one would then have confidence that the dependence of wakefield effects on current shifts up by $1/\alpha$. But such a change in ring impedance is generally not realistic. The Boussard criterion suggests that the threshold to the strong instability depends on $|Z/n|$, but it is known that this is a simplification, that the character of the impedance is also important; and the Boussard criterion says nothing about the weak instability. When reducing an impedance to ameliorate wakefield effects one generally needs to do more careful analysis. For the current SLC damping rings how could we raise the instability threshold? We believe that the instability in the new rings is very sensitive to a small amount of Landau damping. It could be damped by adding a weak, higher harmonic cavity, or by reinserting a small amount of inductance, by *e.g.* introducing a short bellows, or beam pipe with many small holes. However, one must take care not to overdo it, thereby bringing back down the threshold to the strong instability.

Conclusion

We have reviewed our development in understanding of the longitudinal impedance and microwave instability in the SLC damping rings, from the original, to the old, and finally to the current (or new) versions of the ring vacuum chambers. Our calculations were somewhat crude, when compared to what can be done today. Nevertheless, the calculations were a useful complement to measurement, giving reasonable agreement with measurement and insight into the instability, whether in the old, inductive, or new, resistive rings. In the process a new kind of instability–the weak instability–was discovered; it can now be considered to be reasonably well understood.

DAΦNE

Vacuum chamber RF design

The vacuum chamber RF design of the Frascati e^+e^- Φ-factory DAΦNE[38] is a good example of successful benchmarking of impedance codes.

First, the DAΦNE vacuum chamber is complicated. Despite a short collider circumference of about 97 m each ring accommodates all components typical for a multibunch high current collider. The rings contain:

1. two common 10 m long Y-shape interaction regions;
2. four 5 m long narrow gap wiggler vacuum chambers (the wigglers are used for the emittance control and enhancement of the radiation damping);
3. straight sections for allocation of RF cavities, injection kickers, longitudinal feedback kickers, transverse feedback kickers etc;
4. tapers connecting straight sections, bending arcs, wiggler sections, interaction regions;

5. many other components as bellows, flanges, valves, vacuum ports etc.

Second, due to high circulating currents the vacuum chamber was designed to avoid beam instabilities and excessive power losses. New designs and novel ideas were adopted for almost all principal vacuum chamber components: RF cavities [39, 40], shielded bellows [41], longitudinal feedback kickers [42], BPMs [43], DC current monitors [44], injection kickers [45], transverse feedback kickers and others [46]. For example, longitudinal feedback kickers similar to the DAΦNE kicker are routinely used in more than 10 operating colliders and synchrotron radiation sources.

At present, the design single bunch current of 44 mA has been largely exceeded. About 200 mA were stored in a single bunch, while in the multibunch regime 2.4 A of stable beam current were accumulated in the electron ring and about 1.3 A in the positron one.

The following impedance codes were used for impedance and wake field calculations in DAΦNE: ABCI [47], URMEL [48] and OSCAR2D [49] were used in simulations of azimuthally symmetric structures, while the impedance of 3D objects was calculated by MAFIA [20] and HFSS [50]. As a complement to MAFIA and HFSS, the POPBCI code [51] was used to characterize the higher order mode content in the DAΦNE (rectangular waveguide loaded) RF cavity [52].

Impedance bench measurements were carried out for almost all critical vacuum chamber components. Generally, an agreement between the measurement results and the impedance code simulations is satisfactory. Examples of such a comparison are given in a review paper [53], and more details can be found in Refs. [39]-[46].

The total collider impedance estimate obtained with the impedance codes very reliably predicts such important aspects of beam dynamics in DAΦNE as: bunch lengthening, bunch shape and the threshold to the microwave instability.

Bunch lengthening

Bunch lengthening simulations for DAΦNE were performed much before the collider commissioning. The overall short range wake used in the numerical tracking was calculated by adding up contributions of almost all vacuum chamber discontinuities that were estimated analytically or numerically assuming a 2.5 mm gaussian distribution [54], see Fig. 21.

The tracking method is essentially the same as that successfully used in the bunch lengthening simulations for the SLC damping rings [14], SPEAR [25], PETRA and LEP [24]. It consists in tracking the motion of N superparticles in longitudinal phase space over 4 damping times. The turn-by-turn equation of macroparticle motion includes lattice dispersion, radiation damping, stochastic quantum excitation, interactions with the RF field and the wake of all leading macroparticles.

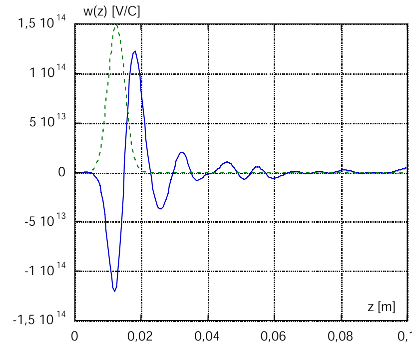

Figure 21: Wake potential of a 2.5 mm long gaussian bunch, which is used in bunch lengthening simulations for DAΦNE.

A comparison between bunch lengthening simulations and bunch length measurements using two different methods is shown in Fig. 22. In the beginning of DAΦNE commissioning a signal from a broadband button was used for bunch length measurements (blue points in Fig. 22). The resulting bunch distribution was found by processing the signal picked up by the button, taking into account the button transfer impedance and the attenuation of the cables connecting the button to a sampling oscilloscope [55]. An example comparison between the simulated bunch shape and the processed signal is shown in Fig. 23.

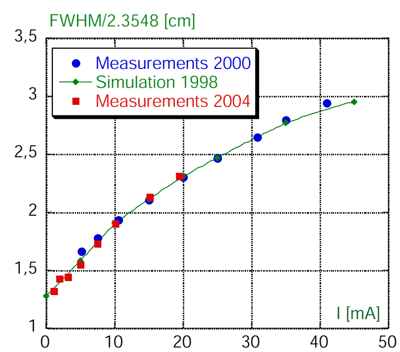

Figure 22: Comparison of bunch lengthening simulations (green line) with bunch length measurements performed with a BPM (blue circles) and a streak camera (red squares).

Later installation of a streak camera made it possible to measure the bunch length in both the electron and positron rings simultaneously [56] (red squares). The bunch profiles at different currents as acquired by the streak camera are shown in Fig. 24. The difference in bunch shape in the two rings is due to an additional inductive impedance in the electron ring: the ion clearing electrodes [57].

The calculated DAΦNE impedance is suitable for predicting bunch behavior not only in the lengthening regime, but also when the short-range wake becomes focusing (bunch shortening). Recently, it has been proposed to use a lattice with a negative momentum compaction factor to

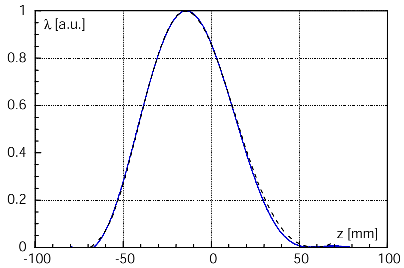

Figure 23: Comparison of the (processed) BPM signal (dotted line) with simulated bunch profile (solid line). The bunch head is to the left.

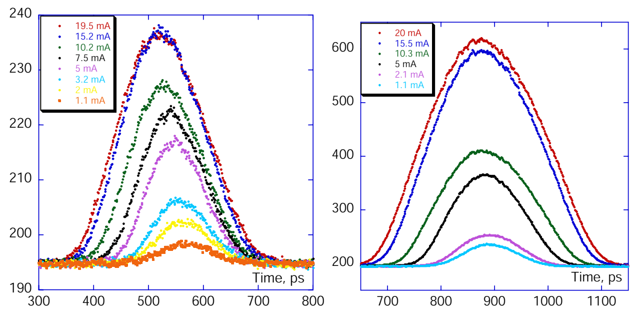

Figure 24: Typical measured bunch distributions in the positron (left) and electron (right) rings. The head is to the left.

increase the luminosity in DAΦNE [58]. For such a lattice the short range wakes are focusing and the bunch shortens until the microwave threshold is reached. An experimental lattice with a negative momentum compaction factor has already been tried in both DAΦNE rings [59]. Fig. 25 shows bunch length as function of current and Fig. 26 gives typical bunch distributions in the positron ring with negative momentum compaction. Again, we can find an agreement between the measurements and the predictions of [58] as far as the bunch length and shape are concerned.

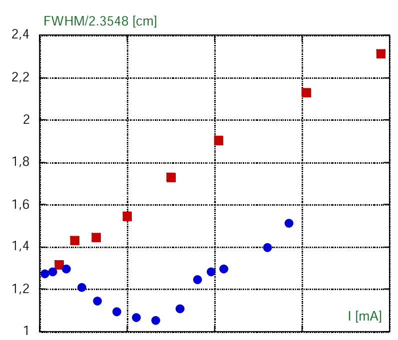

Figure 25: Measured bunch length in the DAΦNE positron ring as function of bunch current for positive (red squares) and negative (blue circles) momentum compaction factor.

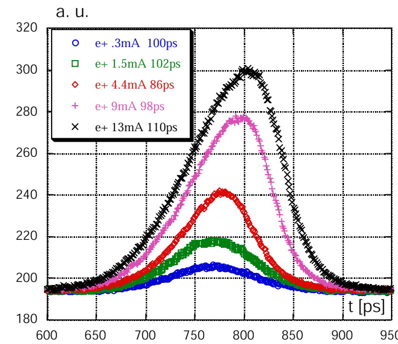

Figure 26: Typical measured bunch distributions in the DAΦNE positron ring with a negative momentum compaction lattice. The head is to the left.

Microwave instability

The coupling between longitudinal coherent modes in a bunch is the driving source of the microwave instability. Different azimuthal modes may couple if their natural frequencies are shifted by amounts comparable to the synchrotron frequency (”strong” instability) while radial modes having the same azimuthal number can couple already for much smaller frequency shifts (”weak” instability). The coherent shift is due to the interaction between the bunch and the machine impedance.

In order to study the microwave instability for DAΦNE again we assumed the machine wake function calculated by the impedance codes shown in Fig. 21. The simple analytical model that we followed treats mode coupling as a splitting of each azimuthal mode in two radial modes. The model is based on approximating the real bunch distribution by a double water bag distribution [34]. By substituting this distribution into the Vlasov equation we solved the resulting eigenvalue system after truncating it (keeping only first 9 azimuthal modes). According to this study, the coupling of radial modes with low azimuthal mode number drives the microwave instability at DAΦNE. For instance, as is seen in Fig. 27, at an RF voltage of 100 kV the lowest thresholds are given by the coupling of radial quadrupole modes at a bunch current of 24 mA and sextupole modes at 28 mA.

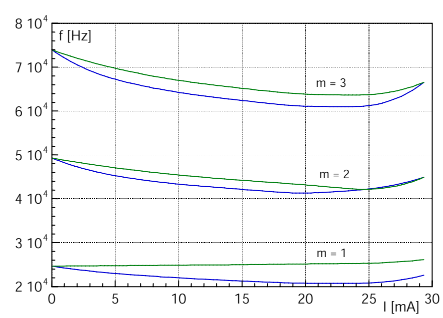

Figure 27: Frequencies of radial bunch modes with lowest azimuthal mode numbers (m = 1, 2, 3) as a function of bunch current.

Experimentally, at a voltage of 100 kV and with the same momentum compaction factor as considered in the analytical model, the quadrupole mode was clearly observed with a spectrum analyzer (see Fig. 28). In the positron ring the threshold current at which the mode signal first appears is about 26 mA, a value that is surprisingly close to the prediction of the simplified analytical model.

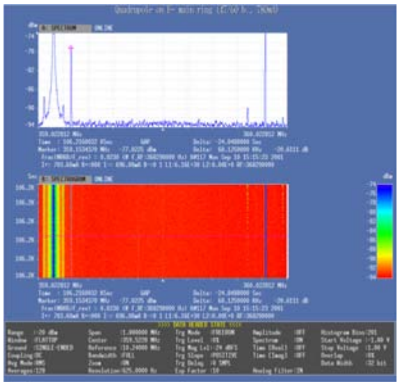

Figure 28: Quadrupole instability sideband as seen on the spectrum analyzer (courtesy A. Drago).

In practise, in the positron ring it was possible to push the threshold to higher currents by varying the RF voltage and increasing the momentum compaction factor. In the electron ring the quadrupole mode instability problem was more severe, presumably due to the higher broad-band coupling impedance. The instability had been limiting the maximum stored current in the e^- ring for a long time, leading to injection saturation, background problems, beam-beam blow up and lifetime reduction. The voltage variation and momentum compaction increase gave only a small increase in the maximum storable current. The problem has been finally solved by tuning the DAΦNE longitudinal feedback system (that initially meant to damp only dipole oscillations) in such a way as to give different longitudinal kicks to the head and tail of bunches [60].

DAΦNE Accumulator Ring

Yet another example of successful impedance code application is the DAΦNE Accumulator Ring, a small booster ring in the DAΦNE injection chain [61]. As in the case of the main rings, the coupling impedance was estimated well in advance of measurements. The longitudinal coupling impedance of 3.5 Ω inferred from the bunch lengthening measurements is in a good agreement with numerical impedance simulations [62]. Fig. 29 shows the calculated wake potential for a 5 mm gaussian bunch, and its Fourier transform (the impedance). Fig. 30 gives a comparison between calculated and measured bunch lengths at different RF voltages and bunch currents.

The measurement of the shift of the transverse betatron tunes and their synchrotron sidebands versus bunch current has shown that the accumulator ring broad-band impedance can be approximated by a $Q = 1$ broad-band resonator

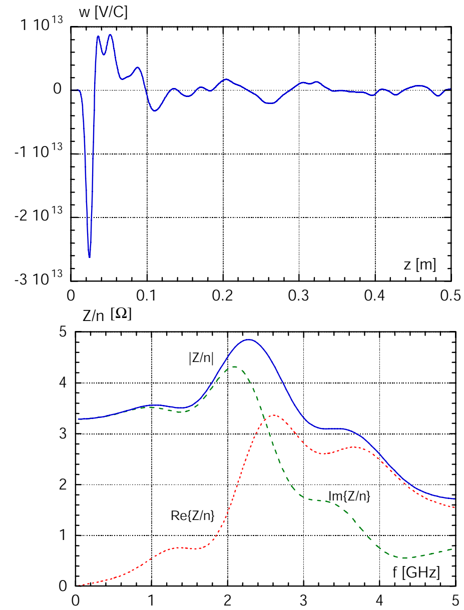

Figure 29: Wake potential of a 5 mm long gaussian bunch (top) and respective FFT transform (bottom) for the DAΦNE Accumulator ring.

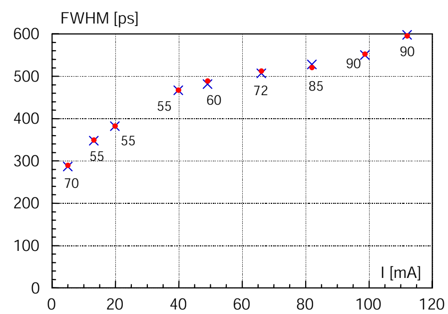

Figure 30: . Bunch lengthening in the DAΦNE Accumulator ring at different RF voltages (red dots - measurement; blue crosses - numerical simulation; numbers correspond to the peak voltage, in kV).

model, with a shunt impedance of 70 kΩ/m [63]. This agrees well with earlier analytical estimates and numerical calculations [64].

APPENDIX: PANEL COMMENTS

Conclusions on impedance codes-MZ

In our opinion, there is no urgent need to develop entirely new software packages for impedance calculations than available today. It would be sufficient to extend already existing tools. The present general-purpose impedance codes, like MAFIA, HFSS, GdfidL and others, have proven their reliability in RF designing and vacuum chamber's impedance optimization. In our paper we have given only a few examples of this.

It does not mean that the existing codes can solve all possible problems arising while calculating the impedance. However, in most cases numerical simulations can be always crosschecked (or substituted) with analytical evaluations and/or experimental measurements results. For particular cases analytical estimates can be helpful in simplifying models to give a possibility of numerical simulations with the existing codes.

Among the practical suggestions for further development of the existing codes we can list a few:

1. possibility to include resistive walls in simulations to take into account:

   - crosstalk between resistive wall and geometric wake fields. Recently this task is getting more important for design of collimation systems for future accelerators, first of all, LHC and linear colliders. - quadrupolar resistive wall wakes responsible of the betatron tune shifts in asymmetric vacuum chambers (measured, for example, in PEP-II, DAΦNE,..)

2. simulations of vacuum chamber elements with thin resistive layers. There are many examples of such components: CTF3 BPMs, DAΦNE ion clearing electrodes, different kinds of kickers etc.

3. further impedance benchmarking is necessary for simulation of components containing frequency dependent materials and/or frequency dependent external loadings

4. possibility of direct impedance calculations at a given frequency.

Comments-KB

Wake Calculation

- As rings become cleaner 3D objects become more important; for short bunch, wakes of long 3D objects are difficult to calculate accurately.

- Short gaussian bunch (used for Green function) filters out high frequencies; what if instability is driven at very high frequencies (*e.g.* CSR, microbunching instability)?

- For short bunch (microbunch), interaction can occur over long distances (catch-up problem).

- Short bunch, long structure, small features: difficult to calculate accurately (mesh dispersion).

  $=>$ improved algorithms: A. Novokhatski (2D, $m = 0$), I. Zagorodnov and T. Weiland (2D, $m > 0$; 3D).

Vlasov Equation Programs

- Oide turned the linearized Vlasov equation into a linear eigenvalue problem; many superfluous stable modes (artifact). Program does not always work.

  $=>$ R. Warnock, M. Venturini, G. Stupakov, turned the linearized Vlasov equation into a nonlinear eigenvalue problem; no superfluous modes. More likely to work for difficult wakes, though does not always work.

Tracking

- Tracking above threshold can yield large fluctuations.

  $=>$ R. Warnock and J. Ellison have developed a program that solves the Vlasov-Fokker-Planck (VFP) equation; more accurate than simple tracking; can *e.g.* solve CSR-driven, microbunching instability; can it be benchmarked with measurements?

ACKNOWLEDGMENTS

We acknowledge the debt of many people who were involved in the SLC and DAΦNE–physicists, engineers, operators–that made it possible to come to some understanding of the ring impedances. We thank also A. Chao, for reading the manuscript and giving useful comments and suggestions; F.-J. Decker, for recent discussion about SLC measurements; R. Warnock and B. Podobedov for supplying figures.

REFERENCES

[1] D. Boussard, CERN LABII/RF/INT/75-2, 1975.

[2] K.L.F. Bane, *et al*, "Impedance Analysis of Bunch Length Measurements at the ATF Damping Ring," in Proceedings of the 10th International Symposium on Applied Electromagnetics and Mechanics (ISEM 2001), Tokyo, 2001.

[3] A. Novokhatski, *et al*, "Transition Dynamics of the Wake Fields of Ultra Short Bunches," in Proceedings of International Computational Accelerator Physics Conference (ICAP 98), Monterey, California, 1998, p. 132.

[4] I. Zagorodnov and T. Weiland, "TE/TM Scheme for Computation of Electromagnetic Fields in Accelerators," Journal of Comp. Physics, 2004 (submitted).

[5] K. Oide and K. Yokoya, "Longitudinal Single Bunch Instability in Electron Storage Rings," KEK-Preprint-90-10, April 1990.

[6] R. Warnock, *et al*, "Linear Vlasov Analysis for Stability of a Bunched Beam," in Proceedings of 9th European Particle Accelerator Conference (EPAC 2004), 2004, p. 2215.

[7] G. Stupakov, private communication.

[8] R. Warnock and J. Ellison, "A General Method for Propagation of the Phase Space Distribution, with Application to the Sawtooth Instability", Presented at 2nd ICFA Advanced Accelerator Workshop on the Physics of High Brightness Beams, Los Angeles, California, 9-12 Nov 1999; SLAC-PUB-8404, March 2000.

[9] Abo-Bakr, *et al*, "Steady-State, Far-Infrared Coherent Synchrotron Radiation Detected at BESSY II," Phys. Rev. Lett. **88**, 254801 (2002).

[10] K.L.F. Bane, *et al*, “Bunch Length and Impedance Measurements in SPEAR,” in Proceedings of 1st European Particle Accelerator Conference (EPAC88), 1988, p. 878.

[11] K.L.F. Bane, “The Calculated Longitudinal Impedance of the SLC Damping Rings,” in Proceedings of 1st European Particle Accelerator Conference (EPAC88), p. 637.

[12] K.L.F. Bane, “Bunch Lengthening in the SLC Damping Rings,” in Proceedings of the Impedance and Bunch Instability Workshop, Argonne, 1989, p. 187.

[13] K.L.F. Bane and C.-K. Ng, “Impedance Calculations for the Improved SLC Damping Rings,” in Proceedings of 1993 IEEE Particle Accelerator Conference (PAC93), p. 3432.

[14] K.L.F. Bane and K. Oide, “Simulations of the Longitudinal Instability in the SLC Damping Rings,” in Proceedings of 1993 IEEE Particle Accelerator Conference (PAC93), p. 3339.

[15] K.L.F. Bane and K. Oide, “Simulations of the Longitudinal Instability in the New SLC Damping Rings,” in Proceedings of 1995 IEEE Particle Accelerator Conference (PAC95), p. 3105.

[16] B.V. Podobedov, “Saw Tooth Instability Studies at the Stanford Linear Collider Damping Rings”, PhD Thesis, SLAC-R-543, June 1999.

[17] A. Hofmann and J.R. Maidment, “Current Dependent Phenomena in LEP,” CERN-LEP-Note 168, 1979.

[18] J. Haïssinski, “Exact longitudinal equilibrium distribution of stored electrons in the presence of self-fields,” Il Nuovo Cimento, **18B**, No. 1, 72 (1973).

[19] A.W. Chao, Physics of collective beam instabilities in high energy accelerators, (John Wiley & Sons, New York, 1993).

[20] R. Klatt, *et al*, “MAFIA - a Three-Dimensional Electromagnetic CAD System for Magnets, RF Structures and Transient Wake Field Calculations”, in Proceedings of the 1986 Linear Accelerator Conference, pp. 276-278, 1986; The MAFIA Collaboration, “User Guide,” CST GmbH, Darmstadt, Germany.

[21] L. Rivkin, *et al*, “Bunch Lengthening in the SLC Damping Rings,” in Proceedings of 1st European Particle Accelerator Conference (EPAC88), p. 634.

[22] A. Renieri, “Turbulence and Bunch Lengthening in Electron-Positron Storage Rings,” Frascati, Report. No. LNF-76/011R, February 1976.

[23] P.B. Wilson, *et al*, “A Computer Simulation of Longitudinal Single Bunch Effects in Electron-Positron Storage Rings,” IEEE Trans. Nucl. Sci., **NS-28**, 2525 (1981).

[24] T. Weiland, “On the Quantitative Prediction of Bunch Lengthening in High Energy Electron Storage Rings,” DESY 81-088, December 1981.

[25] R. Siemann, “Computer Simulation of Bunch Lengthening in SPEAR”, Nucl. Instrum. Meth. **A203**:57, 1982.

[26] D. Brandt, “Simulation of Longitudinal Single Bunch Effects in LEP,” CERN-ISR-TH-89-09, CERN-LEP-NOTE-384, May 1982.

[27] F. Sacherer, IEEE Trans. Nucl. Science **NS-24**, No. 3,1393 (1977); A.W. Chao and J. Gareyte, “Scaling Law for Bunch Lengthening in SPEAR II,” SLAC Report SPEAR-197/PEP-224 (1976) and Part. Accel. **25**, 229 (1990).

[28] P. Krejcik, *et al*, “High Intensity Bunch Length Instabilities in the SLC Damping Rings,” in Proceedings of 1993 IEEE Particle Accelerator Conference (PAC93), p. 3240.

[29] F.-J. Decker, in Damping Rings: Proceedings of the 6th SLAC KEK Linear Collider Workshop, Tsukuba, Japan, 1992, p. 173.

[30] T. Limberg and L. Rivkin, “Damping Rings and Bunch Compression: Summary,” in Proceedings for ECFA Workshop on e^+e^- Linear Colliders (LC 92), Garmisch Partenkirchen, Germany, 1992, p. 357.

[31] M. Minty, private communication.

[32] M. D’yachkov, “Longitudinal Instabilities of Bunched Beams Caused by Short-Range Wake Fields”, University of British Columbia, PhD Thesis, 1995.

[33] K. Oide, “A Mechanism of Longitudinal Single Bunch Instability in Storage Rings”, Part. Accel. **51**: 43-52, 1995; KEK-PREPRINT-94-138, Nov. 1994.

[34] A. Chao, B. Chen, and K. Oide, “A Weak Microwave Instability with Potential Well Distortion and Radial Mode Coupling”, in Proceedings of 1995 IEEE Particle Accelerator Conference (PAC95), pp.3040-3042.

[35] K.L.F. Bane, *et al*, “High-Intensity SIngle Bunch Instability Behavior in the New SLC Damping Ring Vacuum Chamber,” in Proceedings of 1995 IEEE Particle Accelerator Conference (PAC95), p. 3109.

[36] R.L. Holtzapple, “Longitudinal Dynamics at the Stanford Linear Collider”, PhD Thesis, SLAC-R-487, June 1996.

[37] R. Warnock, *et al*, “Simulation of Bunch Lengthening and Sawtooth Mode in the SLAC Damping Rings,” in Proceedings of 7th European Particle Accelerator Conference (EPAC2000), p. 1182.

[38] G. Vignola, “DAΦNE, The Frascati Φ-Factory”, in Proceedings of 1993 IEEE Particle Accelerator Conference (PAC 93), pp. 1993-1997; C. Milardi, *et al*, ”Status of DAΦNE”, Frascati Phys. Ser. **16**: 75-84, 1999.

[39] S. Bartalucci, *et al*, “Analysis of Methods for Controlling Multibunch Instabilities in DAΦNE”, Part. Accel. **48**: 213-237, 1995.

[40] D. Alesini, *et al*, “Third Harmonic Cavity and RF Measurements for the Frascati DAΦNE Collider”, Phys. Rev. ST Accel. Beams **7**: 092001, 2004.

[41] G. O. Delle Monache, *et al*, “DAΦNE Shielded Bellows”, Nucl. Instrum. Meth. **A403**: 185-194, 1998.

[42] A. Gallo, *et al*, “A Waveguide Overloaded Cavity as Longitudinal Kicker for the DAΦNE Bunch-by-Bunch Feedback System”, Part. Accel. **52**: 95-113, 1996.

[43] F. Marcellini, *et al*, “DAΦNE Broad-Band Button Electrodes”, Nucl. Instrum. Meth. **A402**: 27-35, 1998.

[44] M. Zobov, *et al*, “Measures to Reduce the Impedance of Parasitic Resonant Modes in the DAΦNE Vacuum Chamber”, Frascati Phys. Ser. **10**: 371-378, 1998.

[45] A. Ghigo, *et al*, “HOM Damping in the DAΦNE Injection Kicker”, in Proceedings of 7th European Particle Accelerator Conference (EPAC2000), pp. 1145-1147.

[46] M. Zobov, *et al*, “Collective Effects and Impedance Study for the DAΦNE Φ-Factory”, in KEK Proceedings 96-6, August 1996 (A), pp. 110-155.

[47] Y. H. Chin, “User’s Guide for ABCI Version 8.8” (Azimuthal Beam Cavity Interaction”, LBL-35258, UC-414, February 1994.

[48] T. Weiland, “On the Computation of Resonant Modes in Cylindrically Symmetric Structures”, Nucl.Instrum.Meth. **A216**: 329-348, 1983.

[49] P. Fernandes and R. Parodi, “OSCAR2D User’s Guide”, INFN-TC-90-04, Feb 1990. 63pp.

[50] “HFSS, the High Frequency Structure Simulator HP85180ATM.”

[51] P. Arcioni, “POPBCI - a Post Processor for Calculating Beam Coupling Impedances in Heavily Damped Accelerating Cavities”, SLAC-PUB-5444, March 1991.

[52] P. Arcioni, private communication.

[53] F. Marcellini, *et al*, “Beam Coupling Impedance Measurements of the DAΦNE Vacuum Chamber Components”, KEK Proceedings 99-24, February 2000, pp.139-145.

[54] A. Gallo, *et al*, “Single and Multibunch Dynamics Study During the DAΦNE Main Ring Commissioning”, KEK Proceedings 99-24, February 2000, pp. 105-113.

[55] M. Zobov, *et al*, “Bunch Lengthening and Microwave Instability in the DAFNE Positron Ring”, e-Print: Physics/ 0312072.

[56] A. Ghigo, *et al*, “DAΦNE Broadband Impedance”, Proceedings of EPAC 2002, pp. 1494-1496.

[57] B. Spataro and M. Zobov, http://www.lnf.infn.it-/acceleratori/dafne/report/Spataro_Zobov.pdf.

[58] M. Zobov, “Negative Momentum Compaction at DAΦNE”, http://www.lnf.infn.it/conference/d2/TALKS/zobov1.pdf.

[59] M. E. Biagini, *et al*, “Report on DAΦNE MD on 15-16/06/2004”, DAΦNE Technical Note:BM-15, July 12, 2004.

[60] A. Drago, *et al*, “Longitudinal Quadrupole Instability and Control in the Frascati DAΦNE Electron Ring”, Phys.Rev.ST Accel.Beams **6**:052801,2003.

[61] M. E. Biagini, *et al*, “Performance and Operation of the DAΦNE Accumulator”, Proceedings of EPAC 1998, pp. 415-417.

[62] R. Boni, *et al*, “DAΦNE Accumulator Ring Coupling Impedance Measurements”, Nucl. Instrum. Meth. **A418**:241-248, 1998.

[63] M. Zobov, *et al*, “Transverse Mode Coupling Instability in the DAΦNE Accumulator Ring”, DAΦNE Technical Note:G-50, May 1998.

[64] S. Bartalucci, *et al*, “Broadband Impedance and Single Bunch Instabilities”, DAΦNE Technical Note:G-16, January 1993.